Arch. Metall. Mater. **65** (2020), 2, 583-593

DOI: 10.24425/amm.2020.132796

SACHIN SIROHI[1], CHANDAN PANDEY[2*], AMIT GOYAL[3]

A COMPARATIVE STUDY OF TWO NUCLEAR STEEL GRADES WELDED JOINTS

In present work, two nuclear grade steel (P91, P92) are joined using the arc welding process. The welded joints were subjected to the heat treatment in order to restore the mechanical properties and overcome the heterogeneity across the joints. The weldments were studied for microstructure evolution and mechanical behavior under different condition of heat treatment. The variation in mechanical behavior obtained for the welded joints were tried to relate the microstructural evolution. After the normalizing based heat treatment, homogeneity with negligible δ ferrite across the welded joints was observed.

Keywords: Microstructure; GTAW, P91 steel, P92 steel; δ ferrite

1. Introduction

In the present days, the fossil fuel is considered as the primary source of the energy [1]. The need of low pollution emitting and high temperature operating power plants led the development of Cr-Mo steel with other alloying element like V, Nb and B [2]. The new class advanced ferritic-martensitic steel is known as the creep strength enhanced ferritic/martensitic (CSEF/M) steel. The Cr, Mo and W-rich P9, P91 and P92 steel belong to the family of the CSEF/M steels [3]. The successful development and their utilization depend on the weldability. The weldability of the material plays an important role in selection. Hence, weldability of these advanced material become a key issue.

The main factors that affect the weldability of nuclear grade steels are brittle martensitic microstructure, diffusible hydrogen content and residual stresses [4,5]. The trapped diffusible hydrogen content might be responsible for the hydrogen induced cracking [6-8]. However, diffusible hydrogen amount can be controlled by using the low hydrogen welding process and electrode [9,10]. The martensitic microstructure in weld fusion zone can also be tempered using the proper heat treatment. The value of residual stresses mainly developed due to phase transformation and shrinkage and contraction during the welding [11]. The value of residual stresses is also controlled by the heat treatment. However, a low amount of diffusible hydrogen in weld fusion zone or HAZ sometimes combine with either martensitic microstructure or residual stresses leads to the catastrophic failure of the welded joints. Hence, it becomes necessary to use the low hydrogen welding process with proper heat treatment.

The major problem of P91 and P92 steel welded joints are untempered martensitic microstructure formation, uniformity in microstructure across the welded joints, soft zone formation and δ ferrite in weld fusion zone [12-14]. The heterogeneity in mechanical properties across the transverses direction of the welded joint is also responsible for the poor creep rupture strength of the joints. The welded joints of these steels most commonly failed to form the outer zone (boundary line of the base zone and heat affected zone) during the prolonged service condition and referred as the Type IV cracking [15-17]. Both P91 and P92 steel have Cr as primary alloying and around 8.5-9.0% [18,19]. The other alloying elements are V, Nb, W and Mo. The Mo content is used maximum about 0.50% while W is about 2%. In P91 steel, Mo is used about 1%. In P92 steel, boron (B) and tungsten (W) shows a great contribution to creep strength by reducing the coarsening rate of Cr, Mo and W-rich $M_{23}C_6$ precipitates during the creep exposure [20].

The heat treatment aspects of P91 welds have been studied by many of the researcher(s) [21-23]. The primary aim of the heat treatment is to restore the mechanical properties of the soft HAZ and provide softening to the untempered martensitic matrix. The heat treatment also improves the creep rupture strength

[1] DEPARTMENT OF MECHANICAL ENGINEERING, SRM IST DELHI NCR CAMPUS MODINAGAR, UTTAR PRADESH-201204, INDIA
[2] DEPARTMENT OF MECHANICAL ENGINEERING, IIT JODHPUR, KARWAR-342037, INDIA
[3] DEPARTMENT OF MECHANICAL ENGINEERING, SRM IST DELHI NCR CAMPUS MODINAGAR, UTTAR PRADESH-201204, INDIA

* Corresponding author: chandanpy.1989@gmail.com

of the welded joints by minimizing the heterogeneity across it [24]. However, δ ferrite in fusion zone has reported a negligible response to heat treatment [25]. The re-austenitizing based tempering (PWNT) of CSEF/M steels are performed by the Pandey et al. [26] and Manugula et al. [27]. The PWNT treatment was reported superior as compared to the other conventional heat treatment in order to get δ ferrite free uniform microstructure along the welded joint. The Charpy toughness in PWNT treatment was observed equal or more than that of the received material. Abd El-Salamet al. [28] reported the higher creep rupture life and elimination of Type IV cracking in P91 welded joints as a result of the PWNT treatment.

In present work, the P91 and P92 steel plate are joined separately on same process parameters using the gas tungsten arc welding (GTAW) process. A detail investigation of the microstructure in a different zone of the welded joints was explained clearly for different heat treatment.

2. Experimental details

The steel plates of dimensions 100 mm×70 mm×5.5 mm were machined form normalized and tempered (NT) P91 and P92 steel blocks. The schematic of heat treatment performed on P91 and P92 steel plate are depicted in Fig. 1(a). The chemical composition of both the plates is given in Table 1 [14,23].

The plate was welded separately using the GTAW in pure argon (99.99%) environment. For both the welded joints the similar welding process parameters were used. The welding current and arc voltage and welding speed were 230 A, 14 V and 80 mm/min, respectively. The joint was made without groove preparation and to make the intimate contact during the butt welding, plates are surface ground on faces. After the welding, to soften the welded joint two different heat treatments (PWHTs) including (a) post weld heat treatment (PWHT) and, (b) post weld normalizing tempering (PWNT) were performed as per Fig. 1(b). The PWHT condition has been taken from the earlier reported research work. For PWHT, the most commonly used process is tempering at 760°C for 2 h. The similar temperature range and time has also been recommended in AWS and ASME code for P91 welded joint. However, in PWNT treatment, there are two steps and second one (tempering at 760°C for 2h) is similar to the PWHT. The heating rate was 150 °C/ h during the tempering process and it was 200°C/h during the normalizing. For the normalizing, the temperature is selected from the previous work [29-31] The maximum normalizing temperature recommended for the P91 steel was about 1050°C [32] to get the optimum microstructure, and mechanical properties. The purpose of the normalizing is to homogenize the microstructure across the welded joint and produce untempered lath martensite without any ferrite patches. Fig. 2 shows the schematic of the various zone formed in the welded joints.

After the PWHTs, the welded joints subjected to a standard metallographic technique etched in Vilella's solution. The optical and scanning electron microscope was used to investigate the microstructural behavior of the weldments. The Charpy impact tests were performed on standard sub-size specimen (55×10×5 mm^3) at the room temperature and average of three tests has been reported in results. The notches were made in weld fusion zone and HAZ in order to calculate the Charpy toughness of weld fusion zone and HAZ, respectively.

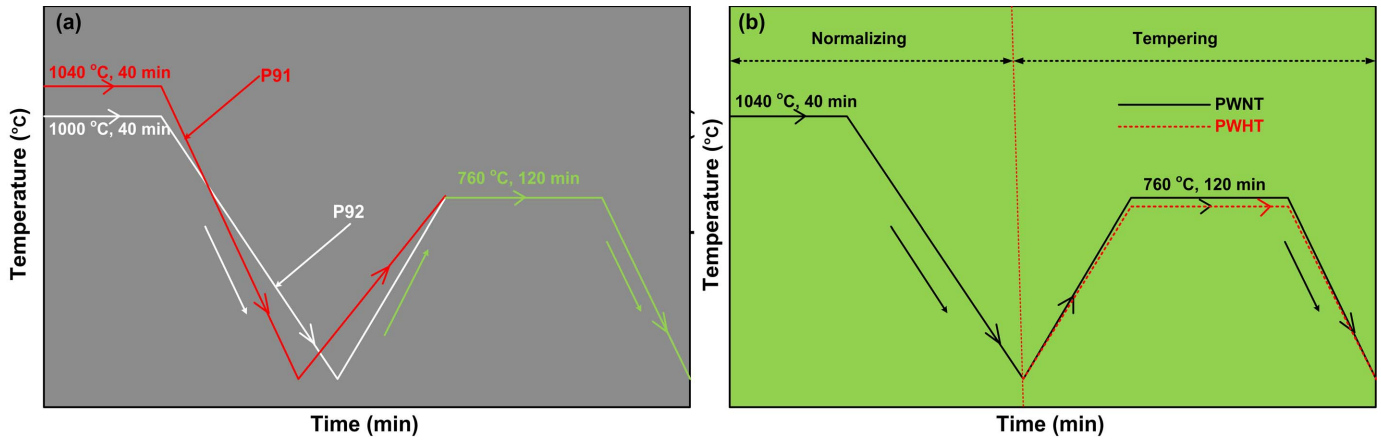

Fig. 1. (a) Schematic diagram for the heat treatment of P91 and P92 steel, (b) schematic diagram used for the post weld heat treatments for P91 and P92 steel welded joints

TABLE 1

Chemical composition of P91 and P92 steel plate (wt. %)

Element	Chemical composition (wt. %)												
	C	Mn	Cr	Si	Mo	V	Nb	Ni	S	Ti	W	Cu	Fe
P91 steel	0.12	0.54	8.48	0.28	0.95	0.18	0.05	0.35	0.011	0.012	<0.001	0.06	Rest
P92 steel	0.11	0.58	9.09	0.48	0.42	0.24	0.07	0.30	0.003	—	1.87	0.03	Rest

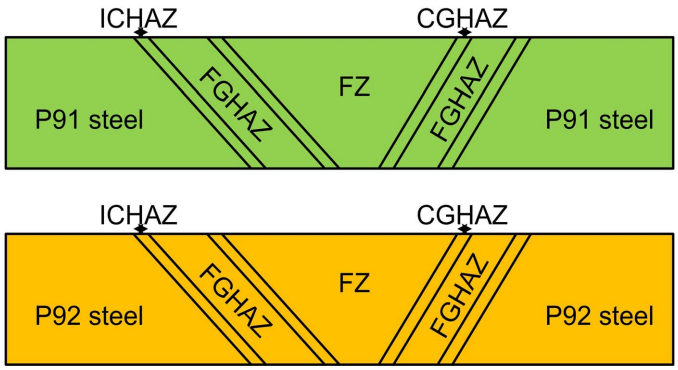

Fig. 2. Schematic diagram of P91 and P92 materials joints with distinct zone

3. Results

3.1. Material characterization

The micrograph of P91 and P92 steel shows the typical tempered martensitic microstructure (Fig. 3). In P91 steel, the prior austenite grain boundaries (PAGBs) and lath boundaries were arrested with the coarse molybdenum and chromium-rich $M_{23}C_6$ type carbide (Fig. 3(e)) while in P92 steel tungsten, molybdenum and chromium-rich $M_{23}C_6$ type (Fig. 3(f)). Fig. 3(a) and (c) reveals the tempered martensitic microstructure with distinct PAGBs and lath blocks as indicated by the lines for both the steels. The coarse PAGs are clearly observed for the

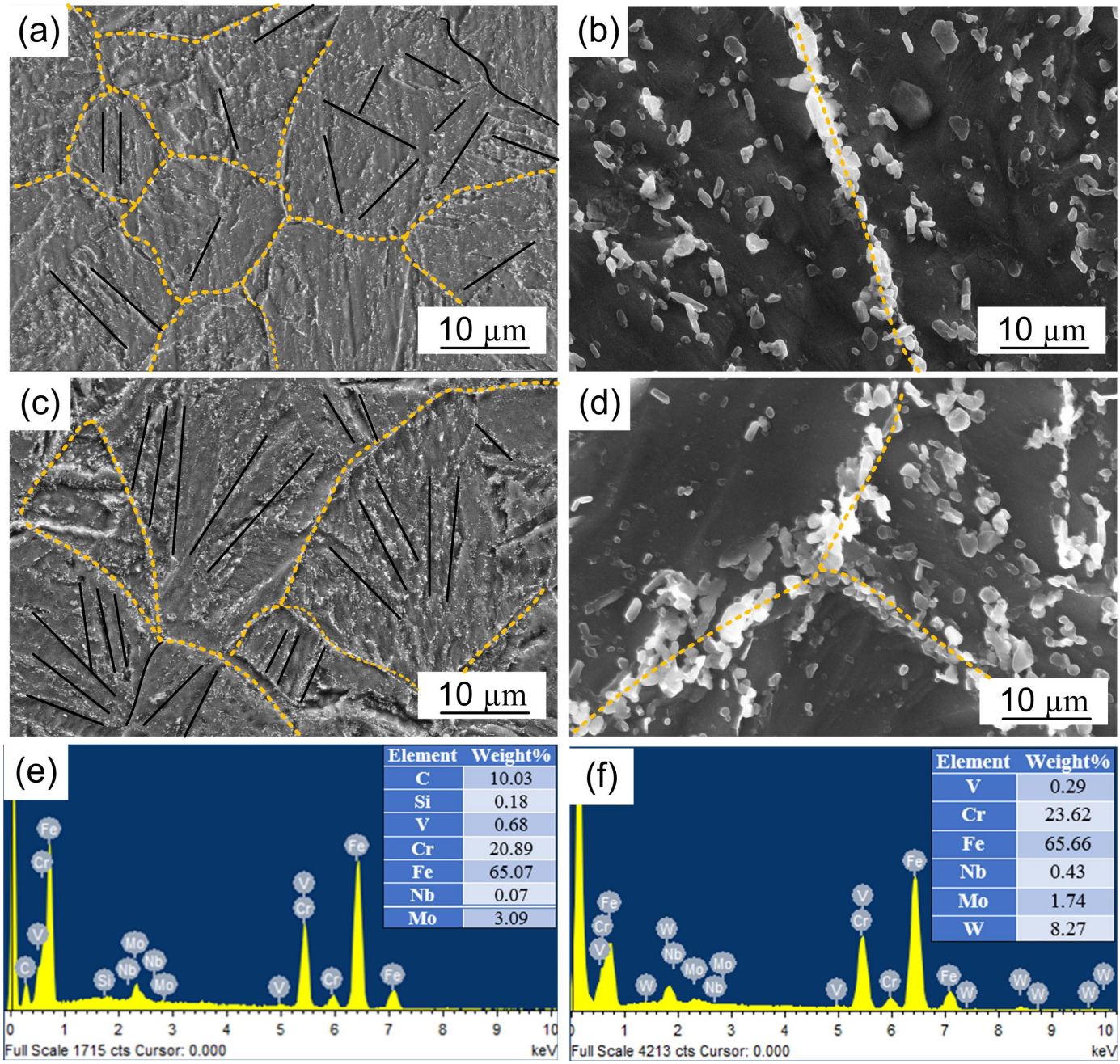

Fig. 3. (a) Micrograph of P91 steel (a) showing PAGBs, lath blocks and precipitates, (b) showing transgranular precipitates; micrograph of P92 steel (c) showing PAGBs, lath blocks and precipitates, (d) showing transgranular precipitates; EDS spectra of precipitates present at the intergranular boundaries for (e) P91 steel, (f) for P92 steel

P92 steel. Fig. 3(b) and (d) shows the distribution of the transgranular V and Nb-rich fine MX precipitates [24]. The average grain size was measured 41±10 and 46±12 μm for P91 and P92 steel, respectively using the ImageJ software. The intergranular coarse $M_{23}C_6$ precipitates helps to resist the grain sliding while fine MX precipitates impede the dislocations movement during prolonged service condition [33-35]. Arivazhagan et al. [29,30] had observed the positive influence of fine MX precipitates on Charpy impact toughness of the base metal while negative on Charpy impact toughness of the welded.

3.2. Microstructure in the as-welded condition

The welding was performed using GTA welding process without filler metal. The higher heat input results in the altering of the base metal microstructure and carbide precipitate free grain boundaries are formed in the fusion zone (FZ). The as-welded microstructure for the P91 and P92 welded joint is shown in Fig. 4. In FZ of P91 welded joints, a fewer amount of δ ferrite zone is formed within untempered martensite laths (Fig. 4(a-b)). However, density and size of the ferrite patches near fusion boundary was high than that of fusion zone (Fig. 4(c)). The similar observation has also been made by Sam et al. [36]. The coarse-grained HAZ that experienced maximum temperature among the HAZs also shows the δ ferrite formation (Fig. 4(d)). The complete dissolution of the $M_{23}C_6$ precipitates in CGHAZ results in the formation of coarse PAGs. The precipitates along the grain boundaries help to resist the movement of it during heat exposure. The coarsening of the precipitates or dissolution of the precipitates leads to the formation of coarse grains as boundaries become free form the pinning effect of precipitates. In fine-grained HAZ (Fig. 4(e)), low peak temperature as compared to CGHAZ is not enough to dissolve all the coarse $M_{23}C_6$ precipitates and results in the formation of fine PAGs with some undissolved precipitates that confirmed form the SEM micrograph.

In P92 welded joints, a completely different microstructure is formed for similar welding process and parameters as a result of differences in chemical composition. The FZ of P92 welded joints shows the higher number density of δ ferrite at a different location. The δ ferrite of different shape and morphology is

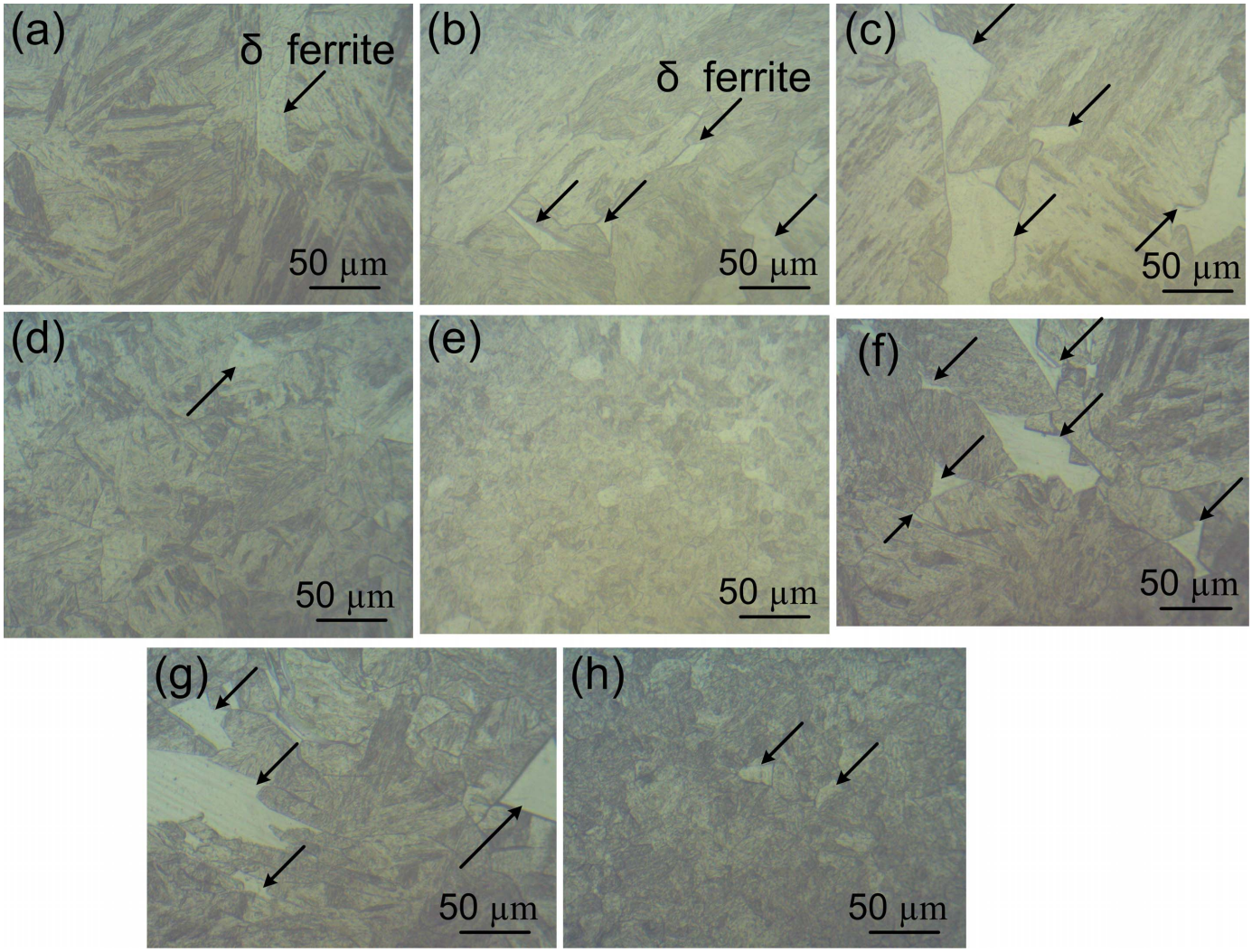

Fig. 4. Optical micrograph of P91 welded joints in as-welded condition (a) fusion zone, (b) fusion zone with δ ferrite, (c) fusion boundary, (d) CGHAZ, (e) FGHAZ; micrograph of P92 welded joints, (f) fusion zone (g) CGHAZ, (h)FGHAZ

clearly seen in Fig. 4(f). Along the weld interface, the number density of δ ferrite is observed higher as compared to FZ. The CGHAZ also shows the presence of δ ferrite with coarse PAGs (Fig. 4(g)). The nucleation of δ ferrite is generally noticed at the PAGBs and it occurred mainly due to the higher density of ferrite stabilizer across the PAGBs. For P92 steel, the δ ferrite is also observed in FGHAZ and attributed to presence of W and Mo in P92 steel composition. The FGHAZ looks similar for both the welded joints except the δ ferrite in FGHAZ of P92 welded joints, as shown in Fig. 4(h). The detail morphology of the δ ferrite patches are shown in Fig. 5.

The SEM micrograph of FZ and FGHAZ both the joints are shown in Fig. 5. The different characteristic of the microstructure is presented with the arrow of a different color. The FZ of the P91 welded joint shows the δ ferrite, lath blocks, and PAGBs (Fig. 5(a)). The number density of δ ferrite was negligible in FZ. The columnar morphology is observed clearly. In FGHAZ, microstructure reveals PAGBs and lath blocks inside the lath packets with a different orientation. The retailed austenite and some undissolved coarse precipitates are also observed. In FZ of P92 welded joint, microstructure reveals the PAGBs, lath blocks and higher density of δ ferrite. The FGHAZ of P92 looks similar to FGHAZ of P91 except for the formation of fine PAGs in P92 FGHAZ. In P92 FGHAZ equiaxed laths are observed (Fig. 5(d)). The welding thermal cycle might be the cause of carbide precipitate free δ ferrite region in FZ of P91 and P92 welded joint.

3.3. Microstructure after the heat treatments

The weld thermal cycle alters the composition of base metal and leads the heterogeneous microstructure formation across the welded joint. To overcome the effect of welding cycle and to get the desirable mechanical properties along the welded joint, it was subjected to the different type of post-weld heat treatments (PWHTs). Effect of PWHTs on micrograph of the distinct zone is shown in Fig. 6.

Micrograph has been taken at a different location of the P91 FZ and it reveals the presence of tempered martensite with some δ ferrite patches, as shown in Fig. 6(a-b). The micrograph of FZ clearly confirms the negligible response of PWHT to δ ferrite. Fig. 6(d) confirms the higher number density of δ ferrite along the joint interface. The FGHAZ and ICHAZ show the tempered martensitic structure with columnar lath patches and coarse precipitates Fig. 6(e-f).

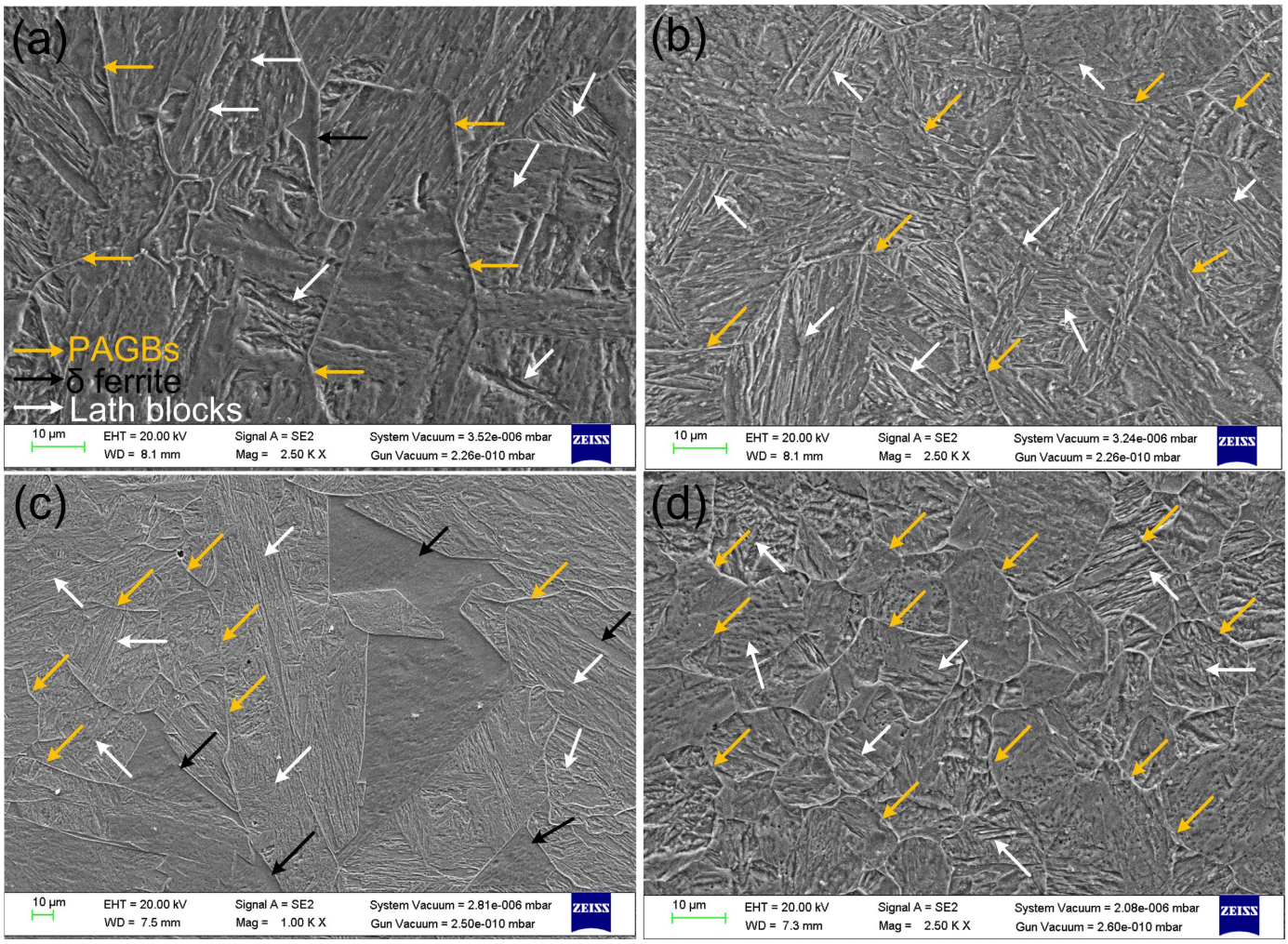

Fig. 5. Micrograph of the P91 welded joint (a) fusion zone, (b) FGHAZ; P92 welded joint (c) fusion zone, (d) FGHAZ

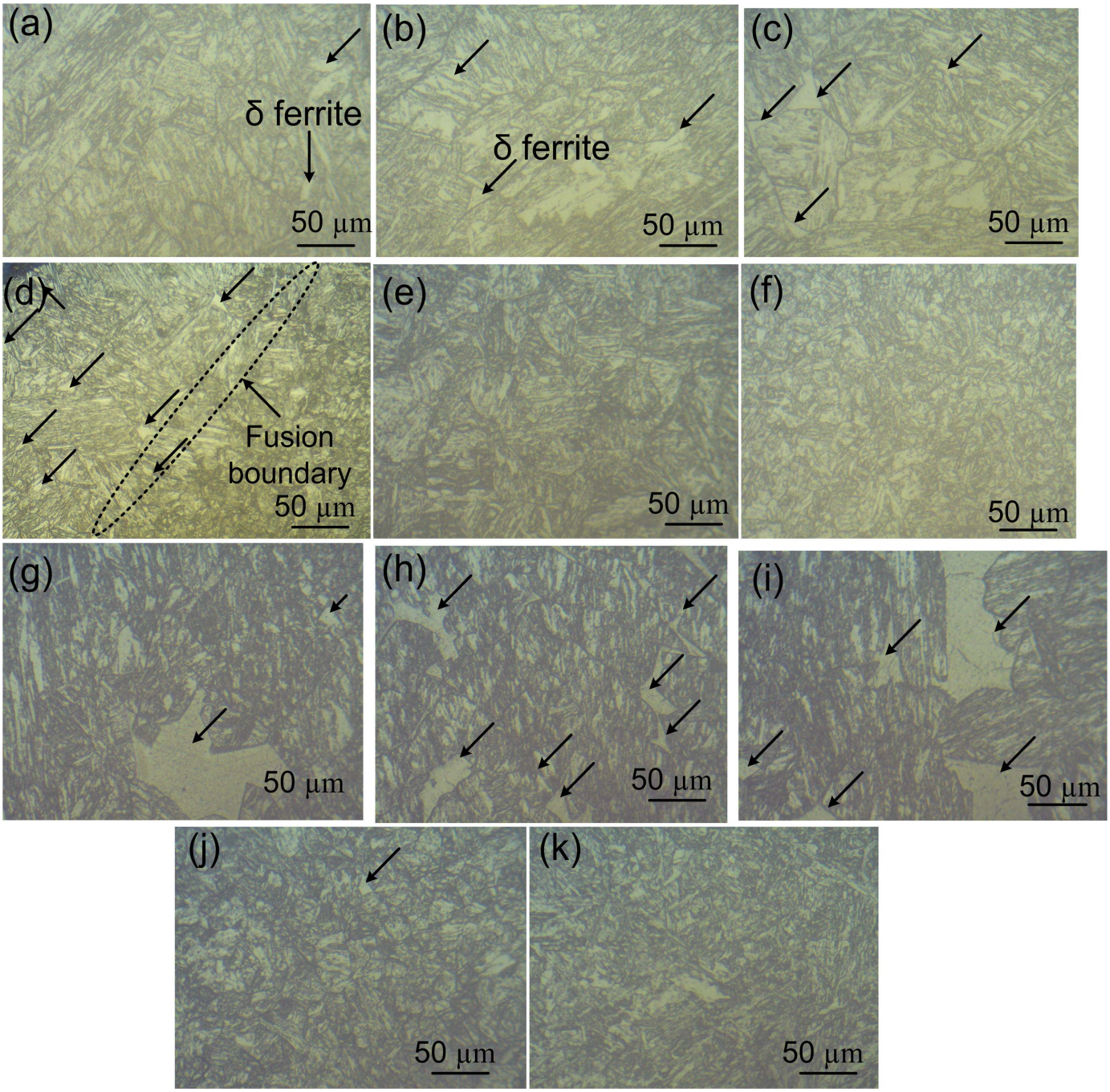

Fig. 6. Optical micrograph of P91 welded joints in as-welded condition (a) fusion zone, (b) fusion zone with δ ferrite, (c) CGHAZ, (d) fusion boundary, (e) FGHAZ, (f) ICHAZ; micrograph of P92 welded joints (g) fusion zone, (h) fusion boundary, (i) CGHAZ, (j)FGHAZ, (k) ICHAZ

The P92 welded joint shows the similar response to PWHT as P91 welded joint and the FZ of P92 welded joint reveals the higher number density and bigger size of δ ferrite (Fig. 6(g)). The interface of welded joint shows the higher number of δ ferrite having small size as compared to FZ and CGHAZ (Fig. 6(h)). The CGHAZ shows the coarse PAGs with δ ferrite near the PAGBs, as shown in Fig. 6(i). The δ ferrite is also observed in FGHAZ but remains absent in ICHAZ (Fig. 6(j-k)). From the microstructural analysis, it is clear that the both FZ and HAZ present in P92 welded joint shows the higher tendency of δ ferrite formation. The SEM micrograph has also been taken to confirm the morphology of δ ferrite after the heat treatment.

The FZ and FGHAZ for the P91 welded joint is depicted in Fig. 7(a) and (b), respectively. The softening occurs after the heat treatment and FZ is characterized with tempered martensite and precipitates. The evolution of precipitates leads to the softening of the matrix as a result of reduction in solid solution hardening. The FGHAZ shows the equiaxed laths with precipitates both along and inside the boundaries. In FZ, coarse PAGs are observed as compared to FGHAZ. The FZ, CGHAZ, and FGHAZ for P92 welded joint are shown in Fig. 7(c), (d) and (e), respectively. The δ ferrite existence is still observed in FZ of the welded joint. The ferrite zone makes the region enriched with ferrite stabilizing element like W, Mo and Cr. At the same time the boundaries

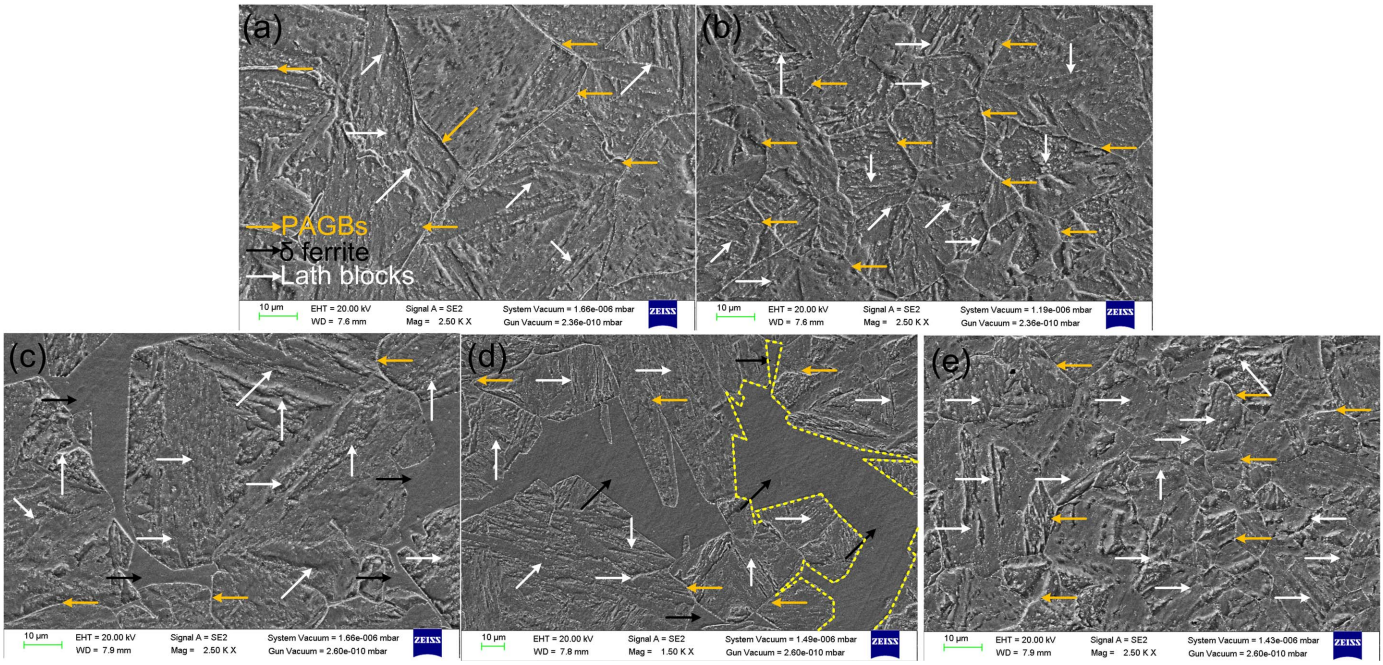

Fig. 7. Micrograph of the P91 welded joint after PWHT (a) FZ, (b) FGHAZ; P92 welded joint (c) FZ, (d) CGHAZ, (e) FGHAZ

become enriched with C and N as a result of ejection from ferrite region. That results in higher density of carbide precipitates along the δ ferrite boundary as compared to PAGBs. The δ ferrite still remains the free from carbide precipitates after the PWHT. The similar observation has also been made by Pandey et al. [37] and Arivazhagan et al. [38]. The CGHAZ shows the δ ferrite region surrounded with the dotted line (Fig. 7(d)). The δ ferrite patches are observed bigger in size as compared to the FZ. In FGHAZ, tempered columnar laths are observed as compared to FGHAZ of P91 welded joint having equiaxed tempered laths.

The micrograph of the distinct zone after the PWNT treatment is shown in Fig. 8. For P91 welded joint, microstructure reveals the over tempered martensite for the each zone. The different zone present in the welded joint looks similar. The austenitizing governs the formation of untempered martensite with dissolution of precipitates. Tempering of the austenitized welded joint resulted in formation of tempered lath martensitic microstructure that looks similar to microstructure of received material. In P92 welded joint, the distinct zone looks similar but having coarse grains as compared to P91 welded joint. Microstructure reveals the tempered martensite with columnar laths inside the PAGBs. The PWNT treatment results in negligible microstructure heterogeneity across the P91 and P92 welded joint. The SEM micrograph has been taken to study the precipitate distribution inside the FZ and HAZ after the PWNT treatment and shown in Fig. 9.

The normalizing temperature in PWNT process is not enough to dissolve all the precipitates present across the PAGBs and they get coarsen during the normalizing process. That results in formation of coarse precipitates along the PAGBs in PWNT treatment process. In FGHAZ microstructure looks similar to the base metal except the precipitate density. In FGHAZ, the precipitate density is observed to be less than that of base metal and FZ (Fig. 9(b)). However, the precipitates inside the intra-lath region still observed with higher number density. The FZ, CGHAZ and FGHAZ for P92 welded joint look completely different as compared to P91 welded joint. However, these zone looks similar for the P92 welded joint with the tempered martensite and $M_{23}C_6$ and MX precipitates. The microstructure of FZ and CGHAZ looks similar to the P92 base zone except the coarse grains in FZ and CGHAZ. In FGHAZ, equiaxed tempered lath martensite with fine PAGs are formed as compared to FZ and CGHAZ. PWNT treatment was resulted in the dissolution of the δ ferrite.

3.4. Charpy toughness of HAZ

To evaluate the Charpy toughness (CT) of the HAZ, a notch was made adjacent to the fusion boundary [21]. The CT of the P91 and P92 base metal were measured 133±6 J and 72±5 J, respectively. The CT of FZ was measured 7.6±4 J for the P91 welded joint and 2.5±5 J for the P92 welded joint. The CT of HAZ was measured 98±6 and 60±5 J for P91 and P92 welded joint. The poor CT of FZ was attributed to untempered martensite having brittle nature as a result of higher carbon percentage. In FGHAZ, the CT was higher than that of minimum required value of 47 J (as per EN 1599:1997). The higher CT of HAZ might be due to partial dissolution of precipitates and results in formation of untempered martensite with lower carbon content. Silwal et al. [39] also reported the higher Charpy toughness for HAZ as compared to FZ in as-welded condition. The PWHT results in the significant improvement in the CT value and it was measured 75±5 and 150±8 J for P92 and P91 HAZ, respectively. The CT of P92 HAZ was measured to nearer of base zone while for P91 HAZ it was much higher than the base zone (133 J). The increase

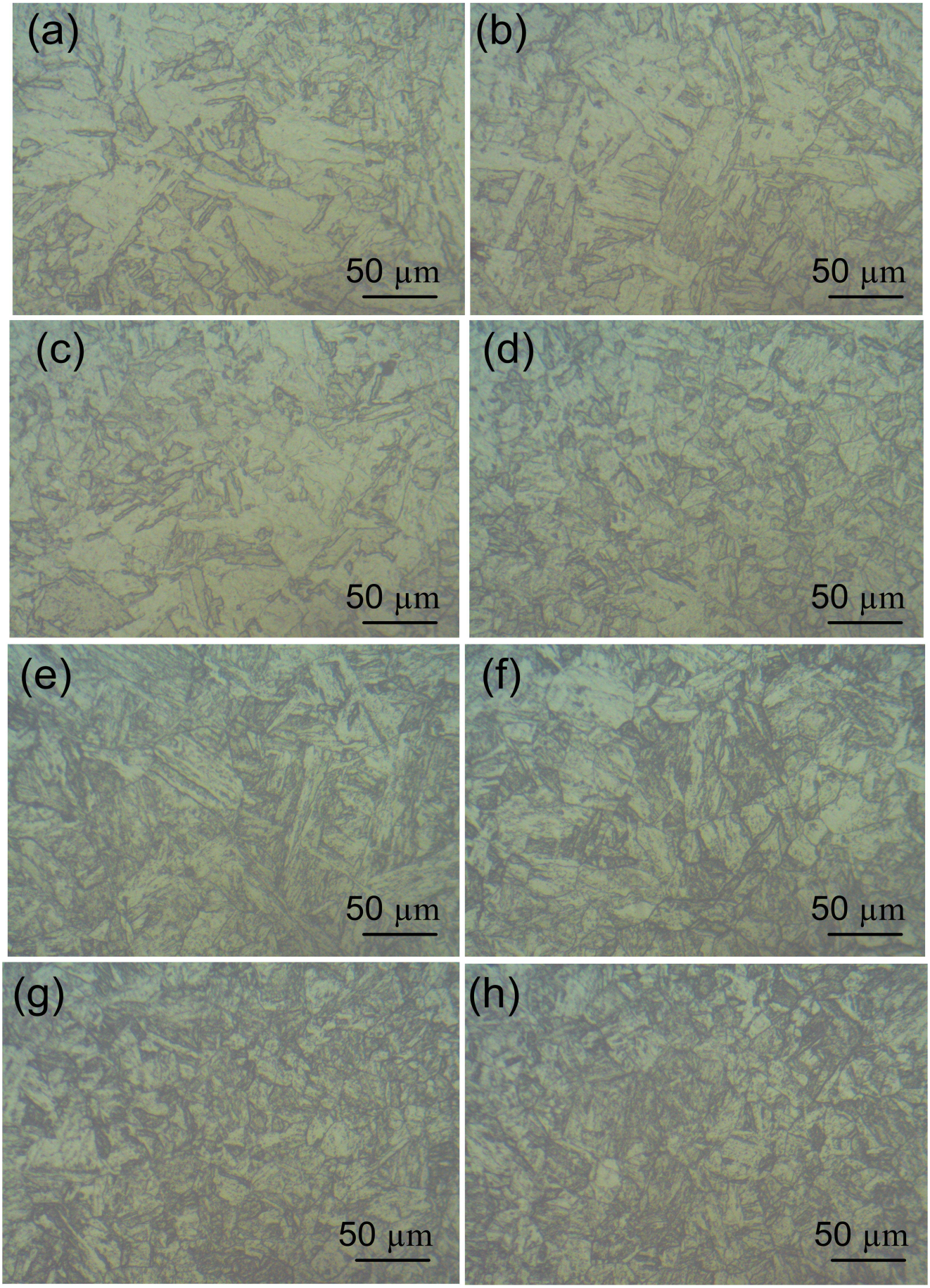

Fig. 8. Optical micrograph of P91 welded joints in as-welded condition (a) fusion zone, (b) FGHAZ, (c) CGHAZ, (d) ICHAZ; micrograph of P92 welded joints (e) FZ (f) FGHAZ, (g) FGHAZ, (h)ICHAZ

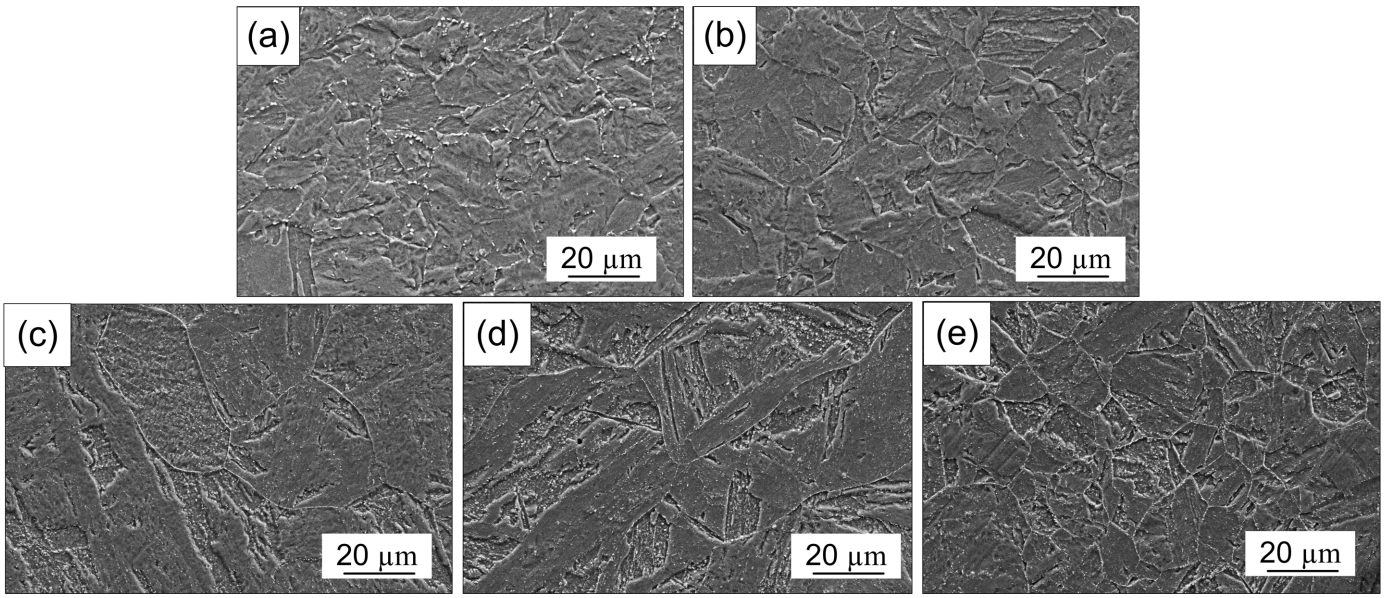

Fig. 9. Micrograph of the P91 welded joint after PWNT (a) FZ, (b) FGHAZ; P92 welded joint (c) FZ, (d) CGHAZ, (e) FGHAZ

in toughness value is attributed to the softening of martensitic matrix. The PWNT results in a drastic increase in the CT value for both the welded joint and it was measured 83±7 and 160±6 J for P92 HAZ and P91 HAZ, respectively. For the PWNT treatment, the higher CT of FZ was also observed by the Pandey et al. [23] for the P91 welded pipe.

4. Discussion

During the solidification or cooling, initially the δ ferrite phase with BCC structure was nucleated from the liquid. On further cooling, the diffusive transformation results in the formation of austenite (FCC) from the δ ferrite (BCC). The formation of δ ferrite at high temperature is governed by the ferrite stabilizing element. At slow cooling rate, generally δ ferrite transformed completely into austenite at Cr concentration about 9%[40]. In P91 and P92 steel welds, NT treatment results in the homogeneous distribution of the Cr in to the matrix. The accumulation of Cr in the matrix about 11.76 wt.% leads δ ferrite content [40]. In HAZ of P91 steel, the lower content of ferrite stabilizer as compared to P92 HAZ that might be cause of formation of duplex structure of α-BCC and δ-BCC in P92 HAZ. The negative influence of δ ferrite on creep rupture strength was reported in earlier research [41-43]. Liu et al. [44] had also reported the higher concentration of the carbide precipitates along the δ ferrite boundaries. The precipitates along boundaries are considered as the undissolved precipitates of base metal during the weld thermal cycle. The precipitates along the boundaries get coarsen during the PWHT and prolonged creep exposure condition. The coarsening of δ ferrite grains might be the cause of local stress concentration that results in the increase in nucleation sites for creep cavities[40]. To enhance the creep rupture properties and eliminate the δ ferrite, PWHT was conducted but it remains unaffected [25]. In order to get the δ ferrite free welded joint, PWNT treatment was conducted and confirms the formation of δ ferrite free welded joint as shown in SEM and optical micrograph. Wang et al. [40] had suggested the heat treatment before the welding process to avoid the δ ferrite. Anderko et al. [45] reported the negative influence of higher δ ferrite on the impact properties. The formation of δ ferrite also results in poor hardness of the FZ. Pandey et al. [12] concluded that the formation of δ ferrite leads the microstructure heterogeneity in FZ. The CT of the P91 and P92 FZ and HAZ had already discussed by the researchers. Silwal et al. [39] had stated that the PWHT is sufficient to get the required CT value in HAZ. However, for the FZ it becomes necessary to increase the time duration of PWHT or temperature. Schafer [46] stated that the higher Cr content in P91 and P92 steel is mainly responsible for the formation of δ ferrite and it also leads to the formation of dendritic carbides. The soft δ ferrite mainly increased the ductility and toughness of the welded joint. However, the combined effect of δ ferrite and dendritic carbide results in the reduction of strength. In present case, the other factor that affects the formation of the δ ferrite is cooling rate. Sam et al. [36] had also stated that the formation of δ ferrite in welded joint is governed by the chemical composition and cooling rate.

4. Conclusions

The P91 and P92 steel welded joint shows the completely different microstructural characteristic and CT value for the heat affected zone (HAZ). The heterogeneous microstructure across the P91 and P92 welded joint were studied in details. The P92 steel showed the higher tendency of the δ ferrite formation in fusion zone (FZ), near the fusion boundary and coarse-grained HAZ (CGHAZ). In P91 steel welded joint, the negligible number density of the δ ferrite is observed in FZ and CGHAZ while it was higher near the fusion boundary. The PWHT results in softening of the martensite matrix while δ ferrite zone did not respond to

PWHT and distinguished as the carbide precipitate free region. The PWHT overcome the microstructure heterogeneity across the welded joint while it still remains. The homogeneous microstructure is obtained for the P91 and P92 welded joint after the post weld normalizing tempering treatment (PWNT). In as-welded condition, the poor CT was observed for the HAZ while it was still higher than the minimum required value. The PWHT results in enhanced value of CT as a result of softening of the martensite. The maximum CT of HAZ was obtained for the PWNT treatment for both the welded joint.

REFERENCES

[1] S.A. David, J.A. Siefert, Z. Feng, Welding and weldability of candidate ferritic alloys for future advanced ultrasupercritical fossil power plants, Sci. Technol. Weld. Join. **18**, 8, 631-51 (2013). 10.1179/1362171813Y.0000000152.

[2] C. Pandey, M.M. Mahapatra, P. Kumar, N. Saini,, Effect of normalization and tempering on microstructure and mechanical properties of V-groove and narrow-groove P91 pipe weldments, Mater. Sci. Eng. A **685**, 39-49 (2016). 10.1016/j.msea.2016.12.079.

[3] R.L. Klueh, D.J. Alexander, E.A. Kenik, Development of low-chromium, chromium-tungsten steels for fusion, J. Nucl. Mater. **227**, 11-23 (1995).

[4] B.J. Mason, K.D. Challenger, Use of implant testing to evaluate the susceptibility of HY-150 steel weldments to hydrogen embrittlement, MS Thesis, Nav. Postgrad. Sch. Monterey, California, 28-9 (1981).

[5] J. Bradley, Use of implant testing to evaluate the susceptibility of HY-130 steel weldments to hydrogen embrittlement (1981).

[6] J. Tomków, G. Rogalski, D. Fydrych, J. Labanowski, Advantages of the application of the temper bead welding technique during wet welding, Materials (Basel). **16**, 6 (2019). 10.3390/ma12060915.

[7] D. Fydrych, A. Świerczyńska, G. Rogalski, J. Łabanowski, Temper Bead Welding of S420G2+M Steel in Water Environment, Adv. Mater. Sci. **16**, 4, 5-16 (2017). 10.1515/adms-2016-0018.

[8] A.S. Aloraier, R.N. Ibrahim, J. Ghojel, Eliminating post-weld heat treatment in repair welding by temper bead technique: Role bead sequence in metallurgical changes, J. Mater. Process. Technol. **153-154**, 1-3, 392-400 (2004). 10.1016/j.jmatprotec.2004.04.383.

[9] A. Świerczyńska, D. Fydrych, J. Łabanowski, The Effect of Welding Conditions on Diffusible Hydrogen Content in Deposited Metal, Solid State Phenom. **183**, 193-200 (2012). 10.4028/www.scientific.net/ssp.183.193.

[10] T. Schaupp, M. Rhode, T. Kannengiesser, Influence of welding parameters on diffusible hydrogen content in high-strength steel welds using modified spray arc process, Weld. World **62**, 1, 9-18 (2018). 10.1007/s40194-017-0535-9.

[11] C. Pandey, M.M. Mahapatra, P. Kumar, N. Saini, Effect of Weld Consumable Conditioning on the Diffusible Hydrogen and Subsequent Residual Stress and Flexural Strength of Multipass Welded P91 Steels, Metall. Mater. Trans. B Process Metall. Mater. Process. Sci. **49**, 5, 2881-95 (2018). 10.1007/s11663-018-1314-8.

[12] C. Pandey, M.M. Mahapatara, P. Kumar, N. Saini, Dissimilar joining of CSEF steels using autogenous tungsten-inert gas welding and gas tungsten arc welding and their effect on δ ferrite evolution and mechanical properties, J. Manuf. Process. **31**, 247-59 (2018). 10.1016/j.jmapro.2017.11.020.

[13] C. Pandey, M.M. Mahapatra, Effect of Groove Design and Post-Weld Heat Treatment on Microstructure and Mechanical Properties of P91 Steel Weld, J. Mater. Eng. Perform. **25**, 7, 2761-75 (2016). 10.1007/s11665-016-2127-z.

[14] C. Pandey, M.M. Mahapatra, P. Kumar, J.G. Thakare Saini, Role of evolving microstructure on the mechanical behaviour of P92 steel welded joint in as-welded and post weld heat treated state, J. Mater. Process. Technol. (2018). 10.1016/j.jmatprotec.2018.08.032.

[15] K. Shinozaki, D. Li, H. Kuroki, H. Harada, K. Ohishi, T. Sato, Observation of type IV cracking in welded joints of high chromium ferritic heat resistant steels, Sci. Technol. Weld. Join. **8**, 4, 289-95 (2003). 10.1179/136217103225005444.

[16] W. Xue, Q. gang Pan, Y. Ren, W. Shang, H. Zeng, H. Liu, Microstructure and type IV cracking behavior of HAZ in P92 steel weldment, Mater. Sci. Eng. A **552**, 493-501 (2012). 10.1016/j.msea.2012.05.076.

[17] S.K. Albert, M. Matsui, T. Watanabe, H. Hongo, K. Kubo, M. Tabuchi, Microstructural investigations on type IV cracking in a high Cr steel, ISIJ Int. **42**,12, (2002) 1497–504.

[18] C. Pandey, M.M. Mahapatra, P. Kumar, N. Saini, Some studies on P91 steel and their weldments, J. Alloys Compd. **743**, 332-64 (2018). https://doi.org/10.1016/j.jallcom.2018.01.120.

[19] N. Saini, C. Pandey, M.M. Mahapatra, H.K. Narang, R.S. Mulik, P. Kumar, A comparative study of ductile-brittle transition behavior and fractography of P91 and P92 steel, Eng. Fail. Anal. **81**, 245-53 (2017). 10.1016/j.engfailanal.2017.06.044.

[20] N. Saini, C. Pandey, M.M. Mahapatra, Characterization and evaluation of mechanical properties of CSEF P92 steel for varying normalizing temperature, Mater. Sci. Eng. A **688**, 250-61 (2017). 10.1016/j.msea.2017.02.022.

[21] C. Pandey, M.M. Mahapatra, Effect of heat treatment on microstructure and hot Impact toughness of various zones of P91 welded pipes, J. Mater. Eng. Perform. **25**, 6, 2195-210 (2016). 10.1007/s11665-016-2064-x.

[22] N. Saini, C. Pandey, M. Mohan, Microstructure Evolution and Mechanical Properties of Dissimilar Welded Joint of P911 and P92 Steel for Subsequent PWHT and N & T Treatment, Trans. Indian Inst. Met. (2017). 10.1007/s12666-017-1145-3.

[23] C. Pandey, M.M. Mahapatra, P. Kumar, A. Giri, Microstructure characterization and Charpy toughness of P91 weldment for as-Welded, post-weld heat treatment and normalizing & tempering heat treatment, Met. Mater. Int. **23**, 5, 900-14 (2017). 10.1007/s12540-017-6850-2.

[24] S.K. Albert, M. Matsui, T. Watanabe, H. Hongo, K. Kubo, M. Tabuchi, Variation in the type IV cracking behaviour of a high Cr steel weld with post weld heat treatment, Int. J. Press. Vessel. Pip. **80**,6, 405-13 (2003). 10.1016/S0308-0161(03)00072-3.

[25] C. Pandey, M. Mohan Mahapatra, P. Kumar, N. Saini, Autogenous tungsten inert gas and gas tungsten arc with filler welding of dis-

similar P91 and P92 steels, J. Press. Vessel Technol. **140**, 2, 1-7 (2018). 10.1115/1.4039127.

[26] C. Pandey, M.M. Mahapatra, P. Kumar, A comparative study of transverse shrinkage stresses and residual stresses in P91 welded pipe including plasticity error, Arch. Civ. Mech. Eng. **18**, 3, 1000-11 (2018). 10.1016/j.acme.2018.02.007.

[27] Vijaya L. Manugula, Koteswararao V. Rajulapati, G. Madhusudhan Reddy, K. Bhanu, Sankara Rao, Role of evolving microstructure on the mechanical properties of electron beam welded ferritic-martensitic steel in the as-welded and post weld heat- treated states, Mater. Sci. Eng. A **698**, 36-45 (2017). 10.1016/j.msea.2017.05.036.

[28] M. Abd El-Rahman Abd El-Salam, I. El-Mahallawi, M.R. El-Koussy, Influence of heat input and post-weld heat treatment on boiler steel P91 (9Cr-1Mo-V-Nb) weld joints: Part 2 – Mechanical properties, Int. Heat Treat. Surf. Eng. **7**, 1, 32-7 (2013). 10.1179 /1749514813Z.00000000051.

[29] C. Pandey, M.M. Mahapatra, P. Kumar, F. Daniel, B. Adhithan, Softening mechanism of P91 steel weldments using heat treatments, Arch. Civ. Mech. Eng. **19**, 2, 297-310 (2019). 10.1016/j.acme.2018.10.005.

[30] C. Pandey, M.M. Mahapatra, P. Kumar, S. Kumar, Effect of post weld heat treatments on microstructure evolution and type IV cracking behavior of the P91 steel welds joint, J. Mater. Process. Technol. (2018). 10.1016/j.jmatprotec.2018.10.024.

[31] C. Pandey, M.M. Mahapatra, P. Kumar, N. Saini, J.G. Thakre, R.S. Vidyarthy, H.K. Narang, A brief study on δ-ferrite evolution in dissimilar P91 and P92 steel weld joint and their effect on mechanical properties, Arch. Civ. Mech. Eng. **18**,3, (2018). 10.1016/j.acme.2017.12.002.

[32] C. Pandey, A. Giri, M.M. Mahapatra, Effect of normalizing temperature on microstructural stability and mechanical properties of creep strength enhanced ferritic P91 steel, Mater. Sci. Eng. A **657**, 173-84 (2016). 10.1016/j.msea.2016.01.066.

[33] M. Yoshino, Y. Mishima, Y. Toda, H. Kushima, K. Sawada, K. Kimura, Phase equilibrium between austenite and MX carbonitride in a 9Cr-1Mo-V-Nb steel, ISIJ Int. **45**, 1, 107-15 (2005).

[34] M. Taneike, K. Sawada, F. Abe, Effect of carbon concentration on precipitation behavior of M23C6 carbides and MX carbonitrides in martensitic 9Cr steel during heat treatment, Metall. Mater. Trans. A **35**, 4, 1255-62 (2004). 10.1007/s11661-004-0299-x.

[35] C.G. Panait, A. Zielinska-Lipiec, T. Koziel, A. Czyrska-Filemonowicz, A.F. Gourgues-Lorenzon, W. Bendick, Evolution of dislocation density, size of subgrains and MX-type precipitates in a P91 steel during creep and during thermal ageing at 600ºC for more than 100,000h, Mater. Sci. Eng. A **527**, 2010, 4062-9 (2010). 10.1016/j.msea.2010.03.010.

[36] S. Sam, C.R. Das, V. Ramasubbu, S.K. Albert, A.K. Bhaduri, T. Jayakumar, E. Rajendra Kumar, Delta ferrite in the weld metal of reduced activation ferritic martensitic steel, J. Nucl. Mater. **455**, 1-3, 343-8 (2014). 10.1016/j.jnucmat.2014.07.008.

[37] C. Pandey, M.M. Mahapatra, P. Kumar, N. Saini, J.G. Thakre, R.S. Vidyarthy, H.K. Narang, A brief study on d-ferrite evolution in dissimilar P91 and P92 steel joint and their effect on mechanical properties, Arch. Civ. Mech. Eng. **18**, 3, 713-22 (2018). http://dx.doi.org/10.1016.

[38] B. Arivazhagan, M. Vasudevan, A comparative study on the effect of GTAW processes on the microstructure and mechanical properties of P91 steel weld joints, J. Manuf. Process. **16**, 2, 305-11 (2014). 10.1016/j.jmapro.2014.01.003.

[39] B. Silwal, L. Li, A. Deceuster, B. Griffiths, Effect of postweld heat treatment on the toughness of heat-affected zone for Grade 91 steel, Weld. J. **92**, 3, 80s-87s (2013).

[40] Y. Wang, L. Zhang, Microstructural analysis of the as-welded heat-affected zone of a grade 91 steel heavy section weldment, Weld. J. **96**, 203-19 (2017).

[41] E.D. Specht, S.M. Allen, Formation of delta ferrite in 9 wt % Cr steel investigated by in-situ X-ray diffraction using synchrotron radiation, Metall. Mater. Trans. A **41**, 2462-5 (2010). 10.1007/s11661-010-0371-7.

[42] S. Kobayashi, K. Sawada, T. Hara, H. Kushima, K. Kimura, The formation and dissolution of residual δ ferrite in ASME Grade 91 steel plates, Mater. Sci. Eng. A **592**, 241-8 (2014). 10.1016/j.msea.2013.10.058.

[43] K. Kimura, K. Sawada, Y. Toda, H. Kushima, Creep Strength Assessment of High Chromium Ferritic Creep Resistant Steels, Mater. Sci. Forum **539-543**, 3112-7 (2007). 10.4028/www.scientific.net/MSF.539-543.3112.

[44] X.Y. Liu, T. Fujita, Effect of chromium on creep rupture properties of a high chromium ferritic heat resistant steel, ISIJ Int. **29**, 8, 680-6 (1989).

[45] K. Anderko, L. Sch, A.K. Ewaiom, Effect of the δ-ferrite phase on the impact properties chromium steels, J. Nucl. Mater. **179-181**, 492-5 (1991).

[46] L. Schafer, Influence of delta ferrite and dendritic carbides on the impact and tensile properties of a martensitic chromium steel, J. Nucl. Mater. **258-263**, 1336-9 (1998).